Modeling the Influences of Pressure and Velocity Variations on the Microwave-Induced Pyrolysis of Wood

R. Tarchini
Dipartimento di Ingegneria Chimica, Università degli Studi di Napoli "Federico II," P.le V. Tecchio, 80125 Napoli, Italy

A. Galgano
Istituto di Ricerche sulla Combustione, C.N.R., P.le V. Tecchio, 80125 Napoli, Italy

C. Di Blasi
Dipartimento di Ingegneria Chimica, Università degli Studi di Napoli "Federico II," P.le V. Tecchio, 80125 Napoli, Italy

DOI 10.1002/aic.12584
Published online March 4, 2011 in Wiley Online Library (wileyonlinelibrary.com).

A detailed two-dimensional mathematical model is studied for the unsteady heat-and mass-transfer equations coupled with a quasi-steady formulation of the electromagnetic field for the microwave-induced pyrolysis of a wood block. The aspects examined include the description of the flow field based on either the assumption of constant pressure and one-dimensional flow velocity directed along the wood fibers or the linked two-dimensional variation of pressure and velocity in accordance with the Darcy law and deviations from the assumptions of local thermal equilibrium between the solid and gas/vapor phase. © 2011 American Institute of Chemical Engineers *AIChE J,* 58: 610–624, 2012
Keywords: fuels, mathematical modeling, wood, microwave, pyrolysis

Introduction

Pyrolysis is a thermochemical technology to convert biomass into more valuable products that can be lumped into three main classes, char, gas, and bio-oil.[1–3] The process is generally made to occur by conventional heating, that is, by means of an external source, which heats the feedstock via conduction, convection, or radiation. Microwave dielectric heating, which takes place through the conversion of the electromagnetic energy into heat within the dielectric medium, offers several advantages with respect to conventional heating, which include:[4] noncontact heating, energy transfer instead of heat transfer, rapid heating, selective material heating, volumetric heating, quick start-up and stopping, heating from the interior of the material body, and higher level of automation. It has attracted a growing interest in the last 20 years with applications in heterogeneous gas-phase catalytic systems[5] and a variety of other fields including food processing, wood drying, plastic and rubber treating, and curing and preheating of ceramics.[6] Consideration has also been given to experimental analysis of biomass pyrolysis induced by microwave heating but after the work of the years 1980',[7–10] only recently a renewed interest has been shown.[11–19] Possible causes for the interruption in these researches can be attributed to the scarce reception of microwave energy by biomass fuels, the need of a multidisciplinary approach to design and develop the related conversion units, the uncertainty about the actual costs, and mainly the lack of highly specific objectives. To improve microwave absorption, microwave receptors are used,[4,12–19] such as carbon materials, inorganic compounds, or water. On the other hand, large sized samples, where the surface heat

Additional Supporting Information may be found in the online version of this article.

Correspondence concerning this article should be addressed to C. Di Blasi at diblasi@unina.it.

losses are smaller than the heat produced by dielectric loss, can be pyrolyzed without the addition of any receptor.[11] Moreover, some improvement in the bio-oil properties[16] with respect to conventional pyrolysis and the specific features of microwave heating outlined above make it very attractive in the framework of integrated biorefineries.[20] Microwave reactors for on-farm processing, to reduce operational costs, have also been proposed such as in the production of biochar for soil applications.[21]

Despite the interest recently shown by several research groups in the experimental analysis about microwave-induced heating of biomass for the thermal processing and production of biofuels and chemicals, the process fundamentals and the complicated interactions between electromagnetic waves and heat/mass transfer across a degrading medium are still largely unknown. Mathematical modeling could contribute to clarify the mechanisms controlling solid conversion and to optimize product yields and composition. Microwave heating of wood has been considered in several cases (for instance, Refs. 22–24) also including moisture evaporation[25] when temperatures are below those needed for the onset of thermal decomposition reactions but only one model[26] is currently available for the microwave-induced pyrolysis of a wood block.

The model[26] consists of two-dimensional partial differential equations for the electromagnetic field and heat- and mass-transfer processes, which are coupled together. More precisely a quasi-steady formulation of the electromagnetic field is coupled with the unsteady equations for the degrading wood, which take into account the chief heat-and mass-transfer mechanisms. Although the model correctly predicts the main experimental features of the microwave-induced pyrolysis of wood, it is still based on the assumption of constant pressure and one-dimensional flow field directed only along the wood fibers.

This study is aimed at investigating the effects of the linked variations of pressure and velocity on the predictions of the microwave-induced pyrolysis of a wood block. Hence, the two-dimensional formulation of the Darcy equation is coupled with the previous formulation[26] of the equations for the heat- and mass-transfer phenomena and the electromagnetic field. Moreover, the effects are examined of the complete or partial deviation from the assumption of local thermal equilibrium between the solid and the gas/vapor phase associated with the complete or partial release of the volatile species at the position where they are produced. The analysis uses the predictions of the field variables and the evaluation of the contribution of the various heat-transfer mechanisms including a comparison with the experimental measurements.

Mathematical Model

In this section, the main assumptions made in the mathematical modeling of wood pyrolysis will be discussed in relation to the schematization of the problem, the formulation of the heat- and mass-transfer equations for the reacting specimen coupled with the equations for the electromagnetic field and the numerical solution method.

Schematization of the problem

The problem simulated is described elsewhere,[26] based on the approximation of a two-dimensional planar field, so only the main characteristics are again discussed here. A schematization of the longitudinal sectional view of the problem has already been reported,[26] where the z axis is parallel to the wood fibers, and the x axis is perpendicular to the wood fibers. A dry wood block is positioned at the bottom of a cavity made of a perfectly conducting material (no loss) where microwaves are supplied by an upper waveguide. In the microwave supply system, a magnetron generates the monochromatic wave of TE_{10} mode with an assigned frequency. The waves, reflected from the cavity walls and wood surfaces, travel backward across the waveguide until modes other than TE_{10} are attenuated. Therefore, the integration domain includes an incident plane, where the incident flux is applied and described as a boundary for the field equations, and an absorbing plane, where the reflected waves are completely undamped. This is described as an absorbing boundary. The incident and the absorbing boundaries delimit the full and the scattered field regions inside the waveguide,[27] respectively. This approach is advantageous because the extent of the computational domain remains finite,[28] and the incident field boundary can be described analytically. The integration domain for the equations of the electromagnetic field consists of the waveguide and the cavity loaded with the wood block. No special boundary conditions need to be implemented at the interface between the empty part of the cavity and the part occupied by the sample. Indeed the variation in the medium dielectric properties is sufficient for describing the presence of the specimen. As a consequence of the position of the wood specimen inside the cavity, the schematized problem is symmetric with respect to the z axis, thus further simplifying the computational treatment of the problem.

The integration domain for the heat- and mass-transfer equations coincides with the wood block, so that boundary conditions are assigned at interfaces with the cavity and the symmetry axis. This schematization is justified by the assumption that the physical and chemical changes undergone by the specimen, as a consequence of microwave heating, do not introduce any modification in the thermal and flow conditions of the empty part of the cavity.

Formulation of the transport and electromagnetic equations

The complete mathematical model for both the heat- and mass-transfer processes and the electromagnetic field is reported in the Appendix A as Supporting Information (with references 29-34). The equations describing the dynamics of the wood block undergoing pyrolysis use the "porous solid approach" of previous models, as extensively discussed in a recent review.[3] In summary, the following main assumptions are made: absence of moisture, constant total volume, negligible mass transport by diffusion, absence of tar vapor condensation inside the pores, ideal gas law, and absence of secondary degradation of tar vapors. Primary degradation is modeled according to the widely used mechanism consisting of three parallel reactions for the formation of three lumped classes of products, char, gas, and tar (oil), with a linear dependence of the reaction rates on the mass fraction of the reacting solid and the usual Arrhenius dependence on temperature. Although the three-step mechanism for the formation of the three classes of pyrolysis products reflects the

current state of the art,[3] secondary reaction effects may become important and should be adequately taken into account in the formulation of more advanced models for the microwave-induced pyrolysis of wood.

The two-dimensional unsteady formulation of the conservation equations takes into account heat transfer by convection and conduction, with the latter described by means of an effective thermal conductivity for the parallel and perpendicular direction of the wood fibers also including a radiative contribution, mass transfer by convection, variation of the void fraction with the conversion level, property (thermal conductivity, specific heats) variation with the temperature, and the conversion level. With respect to the previous model,[26] the assumptions of constant pressure and one-dimensional flow directed as the wood fibers is removed. Instead, the two-dimensional version of the Darcy law for an anisotropic medium is used that links the variable pressure with the flow field.

The two-dimensional version of the Darcy law is expressed by means of the Eqs. 1 and 2:

$$u = -\frac{B_x}{\mu}\frac{\partial p}{\partial x} \tag{1}$$

$$v = -\frac{B_z}{\mu}\left(\frac{\partial p}{\partial z} + \rho_g g\right) \tag{2}$$

where

$$B_x = \eta B_{x\mathrm{W}} + (1-\eta)B_{x\mathrm{C}} \tag{3}$$

$$B_z = \eta B_{z\mathrm{W}} + (1-\eta)B_{z\mathrm{C}} \tag{4}$$

For comparison purpose, the same treatment of the pressure and velocity distribution applied in Ref. 26 is also used. It assumes that the pressure remains constant at the ambient value, p_{atm}, and the flow-field is one-dimensional with the sole component v (directed as the medium fibers). So, Eqs. 1 and 2 are substituted by:

$$p = p_{\mathrm{atm}} \tag{5}$$

$$u = 0 \tag{6}$$

It has been shown[26] that the numerical solution of the Maxwell equations produces characteristic electromagnetic times shorter by several orders of magnitude (about 7–12) than the typical times associated with the rates of wood decomposition and internal and external heat transfer. Therefore, the model adopts a quasi-steady description of the electromagnetic processes, with respect to the unsteady heat- and mass-transfer phenomena for a reacting medium, based on the Helmholtz equation.

Numerical solution method

The solution of the system of partial differential equations, coupling the electromagnetic field with the heat- and mass-transfer processes of degrading wood, is numerically computed in the framework of the software Matlab using a finite difference time domain. The phasor, e_y, and the other field variables of the reacting specimen are centered on the spatial grid, whereas the velocities are positioned at the center of the cell boundaries. The approximation of the Helmholtz equation (Supporting Information Eq. A49) by means of a second-order and space-centered scheme, combined with the Supporting Information algebraic equations Eqs. A50–A53, results in a system of algebraic equations whose coefficient matrix assumes a band form, where the absorbing boundary is treated as in Ref. 35 and the incident boundary as in Ref. 36. Inversion of the matrix, to get the solution, is carried out by a direct method. An upwind scheme for the convective terms and a second-order space-centered scheme are used for the spatial derivatives of the heat- and mass-transfer equations (Supporting Information Eqs. A5–A12) of the reacting specimen, so that a system of ordinary differential equations is obtained. A first-order formula is used to approximate the spatial derivatives in the Darcy equations (Supporting Information Eqs. A29–A30). Then, the odes and the algebraic equations (Supporting Information Eqs. A10, A11, A13–A32 or A10, A11–A13–A28, A47, A48 for the variable or constant pressure case) are solved by means of the routine ode23 of the software Matlab.

The equations for the electromagnetic field and those for the heat- and mass-transfer are coupled owing, on one side, to the dependence of the dielectric properties on temperature and activity of the pyrolysis reactions (the progressive transformation of wood into char, with highly different properties) and, on the other side, to the presence of the local electromagnetic heat generation term Q, in the enthalpy conservation equation, which is directly dependent on the electric field distribution. The electromagnetic field is calculated first with the latest available dielectric properties. Then the solution is used to evaluate the term Q and, thus, the other dependent variables. Given the relatively weak variation of the dielectric properties with temperature, it has also been found that the coupling between the steady electromagnetic field and the unsteady pyrolysis process can be made over time intervals much longer that the time step used to simulate the latter.

Results

The physical properties of the specimen, the kinetic constants and the size of the specimen and the reaction chamber (Table 1), have been selected from previous literature so as to reproduce as closely as possible the experiments.[11] In particular, the permeabilities are those for softwoods,[30] and it is assumed that the ratios between the wood and char permeabilities are the same as in Ref. 38. The simulation, obtained with these data and the variable pressure model, is indicated in the following as reference case.

The spatial grid uses steps along the x and z direction (Δx, Δz) of 10^{-3}m. The solution of the unsteady equations uses a time step of 10^{-2} s (this is determined by a required accuracy level of the solution evaluated in terms of relative and absolute error by the routine ode23 of the software Matlab, assigned equal to 10^{-6} and 10^{-8}, respectively). As the dielectric permittivity of wood is independent of the temperature, the electromagnetic field is not updated until the chemical reactions become active. Then, it is computed over time intervals of 0.5 s. Lower values of the time and space steps and a higher frequency in the upgrading of the electromagnetic field do not introduce any modification in the computed solution.

Table 1. Input Parameters for the Microwave Heating Model of Wood Pyrolysis (Reference Case)

Parameter	Value	Reference
Chemicophysical properties		
A_1	9.28×10^9 (1/s)	37
A_2	1.11×10^{11} (1/s)	37
A_3	3.05×10^7 (1/s)	37
B_{Cx}	11×10^{-14} (m^2)	38
B_{Cz}	48.5×10^{-14} (m^2)	38
B_{Wx}	2.2×10^{-16} (m^2)	30
B_{Wz}	9.7×10^{-14} (m^2)	30
d_C	1.15×10^{-3} (m)	26
d_W	4.0×10^{-5} (m)	30
E_1	1.49×10^8 (J/kmol)	37
E_2	1.77×10^8 (J/kmol)	37
E_3	1.25×10^8 (J/kmol)	37
h_b	100 (W/m^2K)	26
k_{Cx0}	0.071 (W/mK)	39
k_{Cz0}	0.105 (W/mK)	39
k_g	0.026 (W/mK)	39
k_{Wx0}	0.098 (W/mK)	30
k_{Wz0}	0.259 (W/mK)	30
M_G	30 (kg/kmol)	40
M_{N_2}	28 (kg/kmol)	29
M_T	95 (kg/kmol)	40
p_{atm}	1.01×10^5 (Pa)	11
α	1.0	26
ε^*_{W0}	2.4–0.19j	25
$d\varepsilon^*_{C0}$	0.008–0.01j	41
ϕ_0	0.4	30
Δh^0_1	9.36×10^5 (J/kg)	42
Δh^0_2	0 (J/kg)	42
Δh^0_3	-3.52×10^6 (J/kg)	42
ω_W	0.6	43
ω_C	1	43
ρ_{W0}	448.4 (kg/m^3)	11
μ	3×10^{-5} (Pa s)	38
Cavity and specimen specifications		
f	2.45 (GHz)	
F	0.055 (m)	
L_c	0.6 (m)	
L_I	0.086 (m)	
L_S	0.08 (m)	
L_{WG}	0.346 (m)	
P_0	1500 (W)	
W_c	0.3 (m)	
W_S	0.04 (m)	
W_{WG}	0.055 (m)	

In this section, the results are presented of a numerical simulation carried out for a wood block subjected to microwave heating and a comparison is made with both the experimental data[11] and the simulation results of the simplified model based on the assumption of constant pressure and one-dimensional flow.[26] For both cases, an analysis of the various heat-transfer mechanisms is made. Then, a parametric analysis is presented about the influences of the wood and char permeabilities on the characteristics of the conversion process. Finally, the results are discussed about the partial or complete deviation from the assumptions of local thermal equilibrium between the solid and gas/vapor phase and release of volatile products from the external specimen surfaces.

Dynamics of the pyrolysis process

Results of the simulation for the reference case are shown in Figures 1–4 in terms of color maps of temperature, char density, and relative pressure and vector velocity field for times corresponding to conversions of 5, 15, 30, 50, 65, and 75%. The process dynamics are in qualitative agreement with the experimental observation.[11] Induced by microwave heating, decomposition begins in the internal part of the specimen and progressively enlarges toward the external surfaces. At very small conversions (around 2–5%), two zones of relatively high temperature appear, which reproduce the same shape of the electromagnetic intensity. The lower zone is that where the maximum heating rates (4–5 K/s) and the absolute maximum in the temperature (about 1080 K) are attained. Then decomposition becomes active in the upper zone, as testified by the color maps of the char density, also thanks to the contribution of the hot volatile products flowing toward the upper surface at $z = 0.08$ m. Thus, the significant production of volatile species gives rise to maximum component velocity up to 0.10 m/s when the specimen conversion reaches 15%. For this condition, the gas pressure attains a maximum (about 4.5 times the ambient value) nearby the impermeable boundary in contact with the support plate (the absolute maximum is attained at lower conversion, about 5%, and is 5.2 times the ambient value). The values continuously decrease as the upper surface is approached, and the gas/vapor phase products are released in the reaction chamber. The high-pressure values closely to the support plate are justified by the low permeability values of the still unreacted wood.

As conversion increases (30–50%), the pressure always presents the same qualitative distribution, but the maximum is progressively lowered (values of about three times the ambient value) because of the enlargement of the charred region characterized by high permeabilities to gas flow. A further decrease in the maximum pressure is observed at higher conversion, that is, two times the ambient value for a conversion of 65%. The vector velocity field testifies a gas flow directed mainly along the medium fibers, where the permeability is larger by approximately three orders of magnitude. Moreover, the convective transport of heat and mass mainly takes place along the central region of the sample as if a channel is established, as a consequence of the occurrence of the thermal decomposition that collects the volatile mass flow generated from the nearby zones where the resistance to mass flow is still high. For intermediate conversions (30–50%), the flow velocity at the exit region attains values as high as about 0.20 m/s. Deviations from this general trend are shown only for high conversions (above 60%) when, for the most external lateral zones of the specimen, the velocity component along the x direction become the largest and, owing to the large pressures, the flow is released locally, instead of reaching the upper surface at $z = 0.08$ m. An example of the flow field depicting this situation can be seen in Figure 4E for a specimen conversion of 65% when the u component of the velocity vector reaches a value of about 0.20 m/s.

A comparison between the variable and the constant pressure model can be made by comparing the vector velocity field of Figure 4 of the former model with the corresponding plots reported in Figure 5 for the latter model. In addition, the color maps are considered of the temperature at conversions of 5, 15, 30, 50, 65, and 75% (Figure 6) for the constant pressure model.

At a first glance, it appears that for times sufficiently long (conversion above 40%), the shape of the heated and reacted

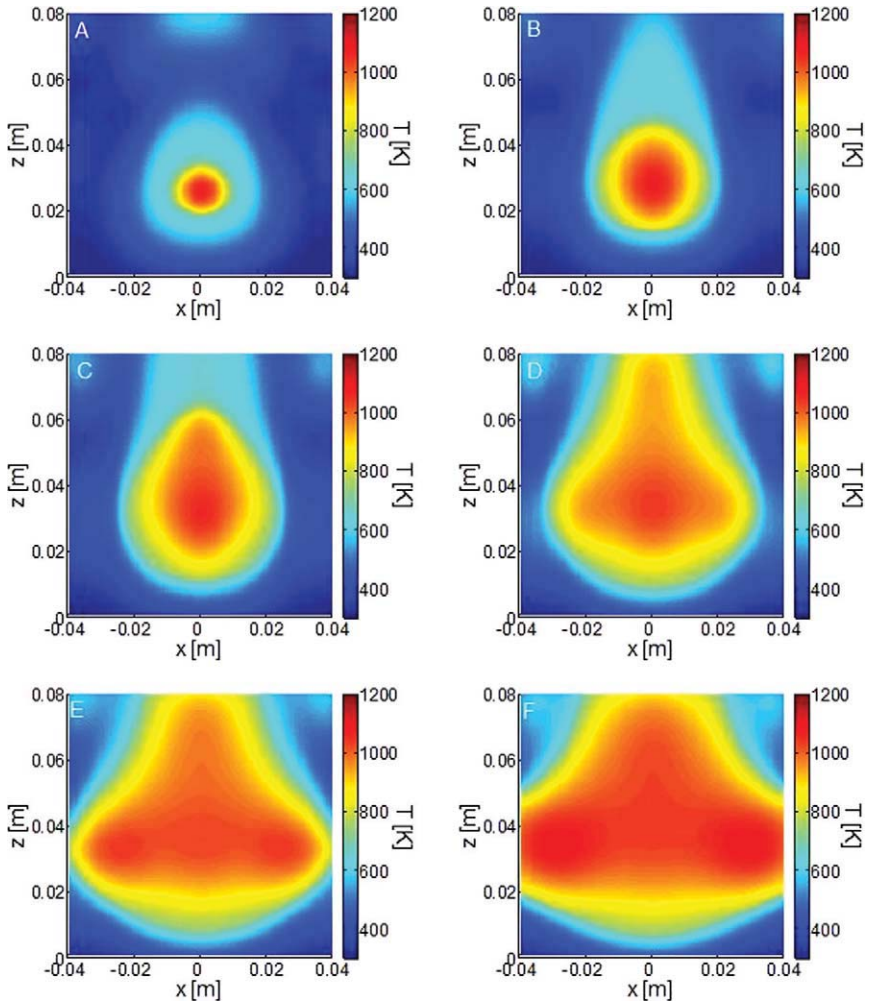

Figure 1. Color maps of temperature, *T*, at conversions of 5% (A, 145 s), 15% (B, 183 s), 30% (C, 229 s), 50% (D, 289 s), 65% (E, 329 s), 75% (F, 361 s) for the variable pressure model (reference case).

[Color figure can be viewed in the online issue, which is available at wileyonlinelibrary.com.]

zone is more rounded for the constant pressure model, a feature that can be explained by the one-dimensional (along the wood fibers) velocity of the volatile decomposition products and the absence of the resistance to mass flow. As shown by the vector field, these assumptions cause that the maximum velocities are not detected along the central reacted zone of the specimen as for the variable pressure model. Instead, maximum velocities are reached where the volatile species are produced and, in general, show higher maxima as the flow of volatile products is distributed over a much narrower section. Thus, at low conversion (i.e., 15%), when the first low zone of high temperatures has already undergone pyrolysis, the maximum velocities (values of 0.37 m/s) are reached at the lateral sides of the reacted zone. Then, at higher conversions (30%), when the second upper zone is degrading, velocities also become high across the central zone of the sample (maxima of 0.43 m/s). The situation of high conversion (50% and above) always reproduce the same qualitative trends observed for low conversion (15%), although the size of the already reacted zone becomes progressively wider and the maxima attain quite high values (up to 0.97 m/s). Thus, the flow of hot volatile products nearby the zones where the volatile products are generated is responsible for the wider and more rounded shape of the heated and already reacted zone predicted by the constant pressure model.

The profiles (not shown) and the color maps of temperature indicate that the differences caused by the two treatments of the flow field have a scarce quantitative influence on the initial process transients (conversion of 30%) when conversion of the lower hot zone takes place. At high conversions, differences remain small along the lower and almost completely reacted region ($z < 0.05$ m) and become progressively larger along the upper part of the integration domain. The localization of the higher v component of the velocity vector along the central zone of the specimen for the variable pressure model gives rise to higher temperatures in the direction of the fibers. This trend is already evident for conversion of 30% and, given the dependence of the dielectric properties on temperature (besides the conversion level) causes larger ε' and ε'' values (not shown).

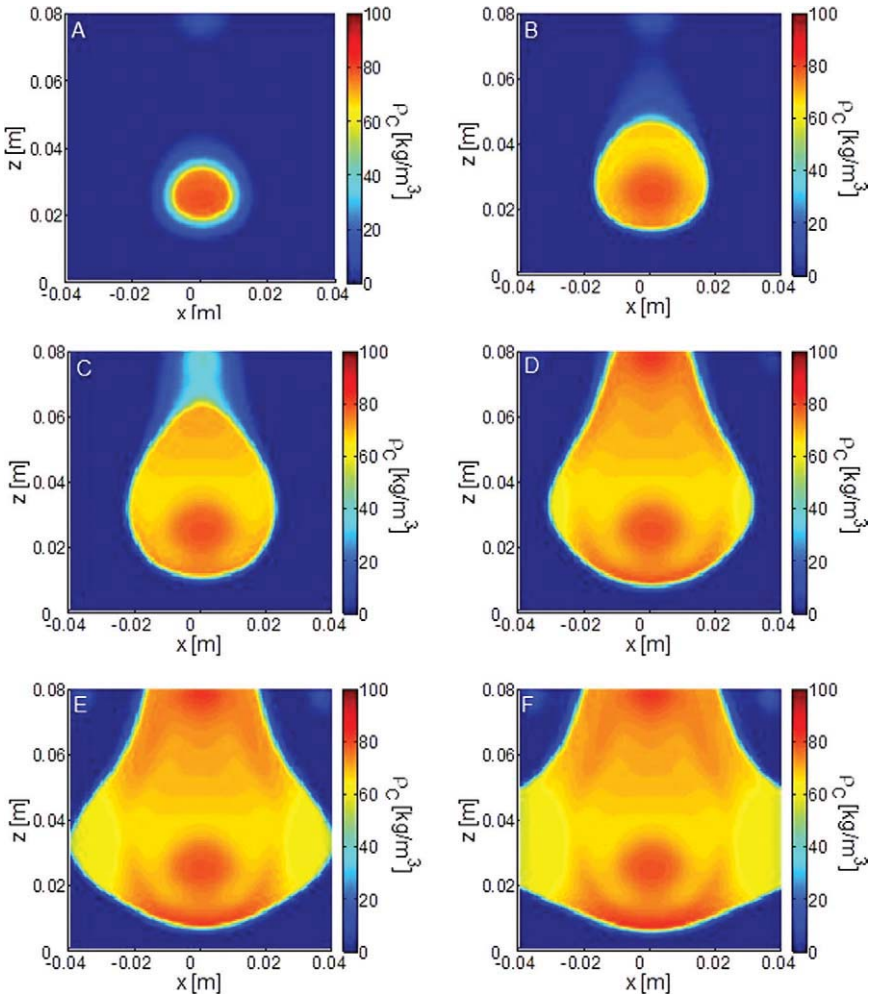

Figure 2. Color maps of char density, ρ_C, at conversions of 5% (A, 145 s), 15% (B, 183 s), 30% (C, 229 s), 50% (D, 289 s), 65% (E, 329 s), 75% (F, 361 s) for the variable pressure model (reference case).

[Color figure can be viewed in the online issue, which is available at wileyonlinelibrary.com.]

The color maps of the tar density (not shown) indicate that for the constant pressure model, values are lower nearby the bottom impermeable boundary. In other words, the assumption of constant pressure also modifies the residence times of the tar vapors inside the hot degrading medium. Although not described by the present model, the activity of secondary reactions is consequently modified at a certain extent.

Further comparison between the two models can be made by means of the temporal profiles of the weight loss curves (Figure 7) and some characteristic parameters, reported in Table 2, which include the yields of the three product classes (Y_C, Y_T, and Y_G) expressed on a dry mass basis, the induction time, t_i, defined as the time when a conversion 5% is reached, the inflection time, t_{infl}, defined as the time when, after the absolute maximum, the slope changes of the rate of weight loss, and the corresponding solid mass fraction, Y_{infl}, the conversion time (conversion of 95%), t_c, the maximum volatile release rate, dY_{vm}, and the corresponding time, t_{vm}, and the maximum relative pressure, p_{max}/p_{atm}, and the corresponding time, $t_{p_{max}}$. Figure 9 also reports the experimental data.[11] From the qualitative point of view, the weight loss curves present three local maxima (also appearing in the curve of the dissipated power, not shown) corresponding to the decomposition of the first hot zone located in bottom region of the sample, the second hot zone located in the upper part of the sample and finally the enlargement of the reaction zone.

Weight loss curves also show that three main periods characterize the dynamics of the conversion process: an induction period, defined as above (conversion of 5%), a central period of rapid weight loss, ($t_{infl} - t_i$), and a final tailing zone, ($t_c - t_{infl}$). The induction period (time of 145–146 s) is not affected by convective heat and mass transfer, which is not yet active, so there are no differences between the two models. Differences are also negligible for the initial part of the central period (up to times of 230 s and conversions around 30%). Then, the predictions of the two models become different. It can be noted that the maximum rate of volatile release is significantly higher for the constant pressure model (4.7×10^{-3} s^{-1} vs. 3.5×10^{-3} s^{-1}). Consequently, the period of fast rates of volatile release is longer (301 vs. 229 s with an increase of about 31%) for the

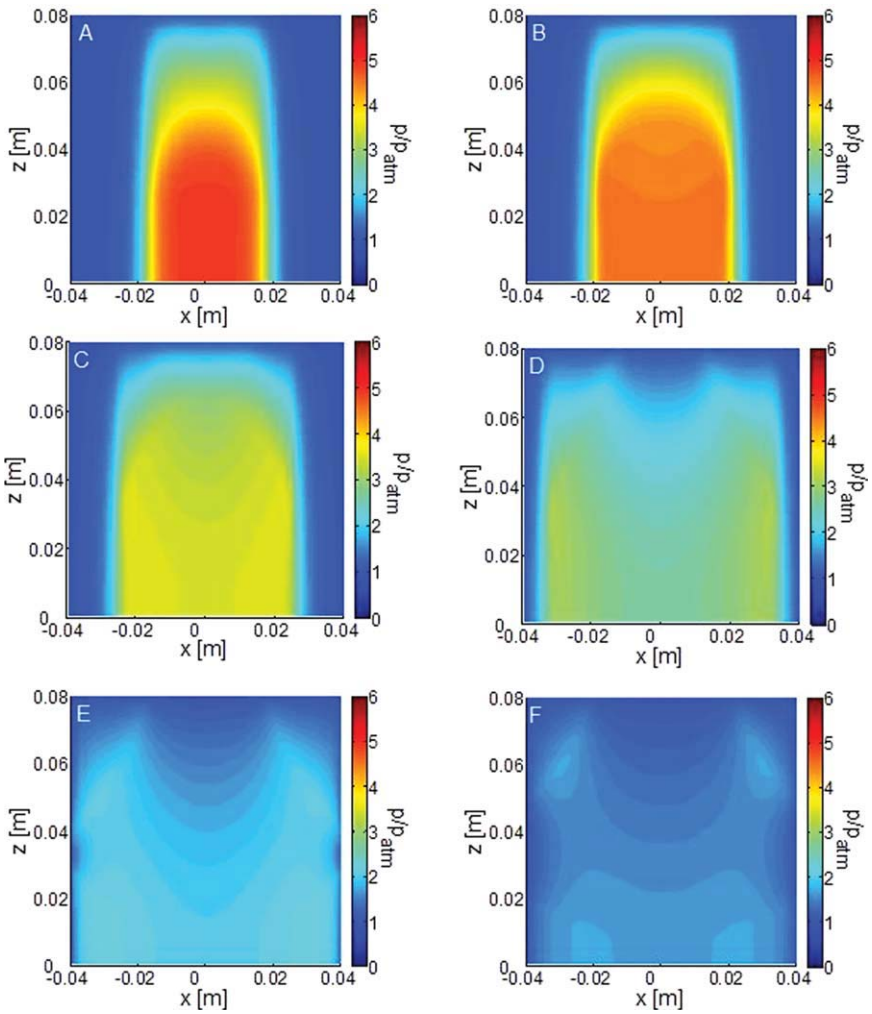

Figure 3. Color maps of relative pressure, p/p_{atm}, at conversions of 5% (A, 145 s), 15% (B, 183 s), 30% (C, 229 s), 50% (D, 289 s), 65% (E, 329 s), 75% (F, 361 s) for the variable pressure model (reference case).

[Color figure can be viewed in the online issue, which is available at wileyonlinelibrary.com.]

variable pressure model owing to the less efficient heating of the unreacted wood from the hot volatile products, as they mainly flow along the central zone of the specimen. The opposite trend is observed for the final tailing zone where the variable pressure model reaches the conversion conditions at times significantly shorter (duration of 98 s vs. 221 s with a reduction of about 56%) resulting from the convective heating also for the direction perpendicular to the wood fibers.

In accordance with the process dynamics already described, the quality of the agreement between the model prediction and the experiments for the initial transients is not significantly dependent on the description of the velocity vector and relative pressure field. For long times, the variable pressure model shows a better agreement.

Heat-transfer mechanisms

To evaluate the role played by the different heat-transfer mechanisms and the importance of the description of the pressure and velocity field on the predictions of microwave-induced pyrolysis, the energy conservation equation is integrated over the computational domain to get[38]:

$$\int_0^{L_S}\int_0^{W_S} \frac{\partial(\rho_S h_S + \phi\rho_g h_g)}{\partial t}\,dxdz = Q_{cx} + Q_{cz} + Q_{kx} + Q_{kz} + Q_r + Q_m \quad (7)$$

In the Eq. 7, Q_{cx} and Q_{cz} are the contributions due to convection (x, z), Q_{kx} and Q_{kz} those due to conduction (x, z), Q_r the total reaction enthalpy, and Q_m the microwave energy generation term:

$$Q_{cx} = \int_0^{L_S} (-\alpha u \rho_g h_g)\big|_{x=W_S} dz \quad (8)$$

$$Q_{cz} = \int_0^{W_S} (-\alpha v \rho_g h_g)\big|_{z=L_S} dx \quad (9)$$

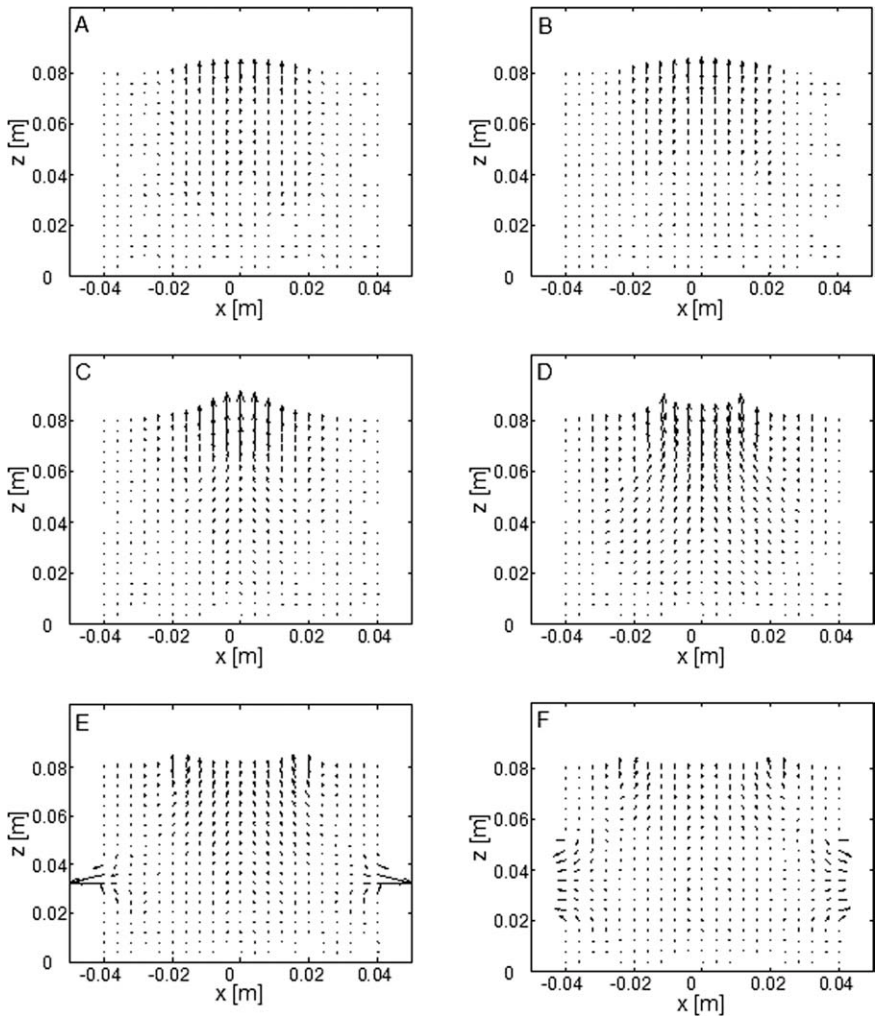

Figure 4. Vector velocity field for the constant pressure model.

Vector velocity field at conversions of 5% (**A**, 145 s, maximum velocity 0.094 m/s), 15% (**B**, 183 s, maximum velocity 0.102 m/s), 30% (**C**, 229 s, maximum velocity 0.192 m/s), 50% (**D**, 289 s, maximum velocity 0.198 m/s), 65% (**E**, 329 s, maximum velocity 0.197 m/s), 75% (**F**, 361 s, maximum velocity 0.108 m/s) for the variable pressure model (reference case).

$$Q_{kx} = \int_0^{L_S} \left(k_x^* \frac{\partial T}{\partial x} \right)\Big|_{x=W_S} dz \tag{10}$$

$$Q_{kz} = \int_0^{W_S} \left(\left(k_z^* \frac{\partial T}{\partial z} \right)\Big|_{z=L_S} - \left(k_z^* \frac{\partial T}{\partial z} \right)\Big|_{z=0} \right) dx \tag{11}$$

$$Q_r = \int_0^{L_S} \int_0^{W_S} -\left(K_1 \Delta h_1^0 + K_2 \Delta h_2^0 + K_3 \Delta h_3^0 \right) dx dz \tag{12}$$

$$Q_m = \int_0^{L_S} \int_0^{W_S} Q dx dz \tag{13}$$

The contributions defined by Eqs. 8–13 are plotted in Figures 8A–C as functions of time. As expected, the microwave energy generation term reaches the absolute maximum and is always preponderant with respect to the contribution given by the other mechanisms. Moreover conductive and convective heat transfer take place from the internal region of the sample toward the most external region, so the relative contributions are negative. The reaction enthalpy also testifies a process globally endothermic although this contribution is comparatively smaller. During the induction period, all the contributions are small except Q_m. Then, for the fast weight loss rate period, the convective contribution along the medium fibers becomes successively more important. It is worth noting that the hot gas and vapors produced from the reaction transfer heat outside the sample introducing the so-called convective cooling.[3] However, contrary to the case of conventional heating where the flow is directed along the already charred region, in the case of microwave heating, the flow of hot volatile products across still virgin wood cause some preheating, thus reducing the heat amount released to the environment.

The variable pressure model shows slightly higher values of Q_m. Also, Q_{cz} is initially slightly higher. Then an abrupt decay is shown, corresponding to the appearance of the

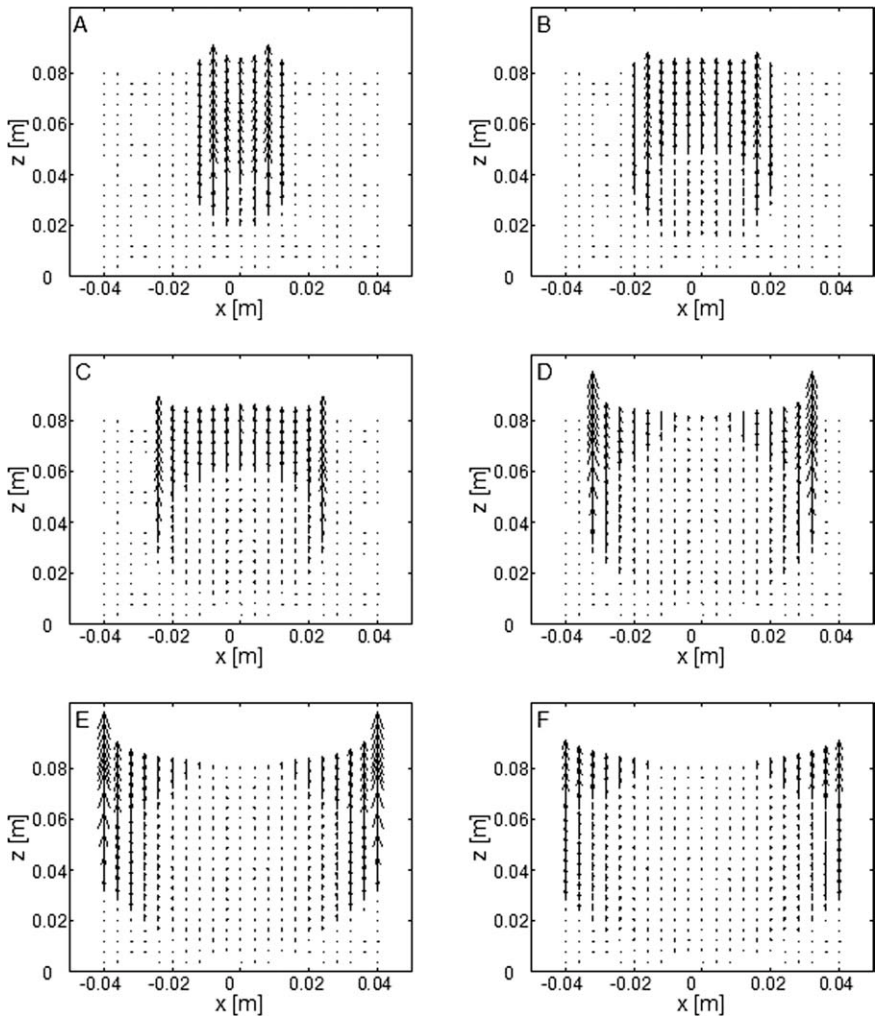

Figure 5. Vector velocity field for the constant pressure model.

Vector velocity field at conversions of 5% (**A**, 146 s, maximum velocity 0.35 m/s), 15% (**B**, 183 s, maximum velocity 0.37 m/s), 30% (**C**, 228 s, maximum velocity 0.43 m/s), 50% (**D**, 279 s, maximum velocity 0.64 m/s), 65% (**E**, 309 s, maximum velocity 0.97 m/s), 75% (**F**, 331 s, maximum velocity 0.2 m/s) for the constant pressure model.

component Q_{cx}, which is completely absent from the constant pressure model and associated with a change in the structure of the vector velocity field already discussed. A rapid decay in the components of the convective heat transfer is observed at the conclusion of the period of rapid weight loss. It can be observed that in terms of absolute value, the maximum in the Q_{m} is more than double with respect to that in Q_{cz}. However, it can be assumed that apart from the expected importance of the microwave terms, the period of rapid weight loss is significantly affected by the convective transport.

The rate of heat conduction assumes negligible values during the induction period and starts to become significant at about the half of the second period of rapid weight loss. It attains its maximum when this period comes to an end and maintains high values during the entire duration of the last tailing zone. Therefore, the third slow period in the microwave pyrolysis dynamics, apart again the microwave energy term, is dominated by heat conduction. As already anticipated, the absence of convective transport, along the x direction, for the constant pressure model is responsible for the longer duration of this period.

Effects of the medium permeabilities

The influences of the wood and char permeabilities to gas flow, B_{W} and B_{C}, are investigated by increasing or decreasing five times their values with respect to those of the reference case listed in Table 1. Simulations show that as the permeability of wood is increased, the qualitative features of the process tend to resemble those already described for the constant pressure model. As the permeability of char is increased, the flow of volatile pyrolysis products along the central region of the specimen, where pyrolysis has already occurred, is successively more favored. Hence, the qualitative features of the process always remain similar to those already discussed for the variable pressure model. A list of the predicted process parameters is reported in Table 3. As expected, the induction period is independent of the permeability values. The duration of the period of rapid weight

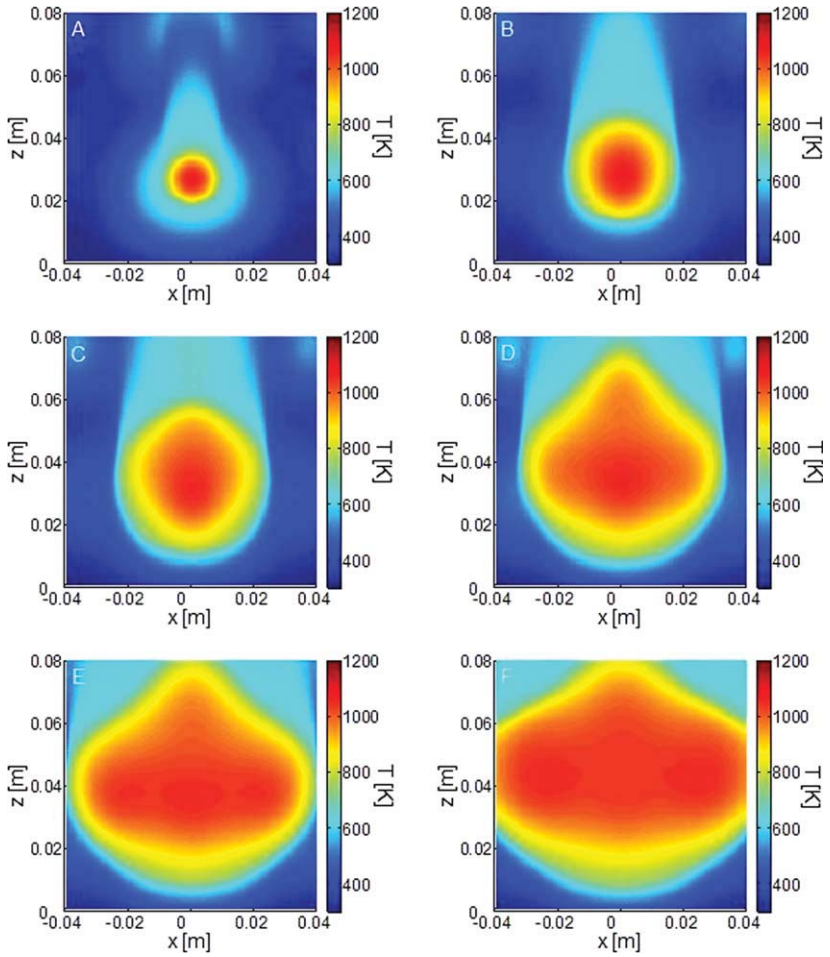

Figure 6. Color maps of temperature, *T*, at conversions of 5% (A, 146 s), 15% (B, 183 s), 30% (C, 228 s), 50% (D, 279 s), 65% (E, 309 s), 75% (F, 331 s) for the constant pressure model.

[Color figure can be viewed in the online issue, which is available at wileyonlinelibrary.com.]

loss become shorter as B_W is increased or B_C is decreased. For variations by a factor of five, the quantitative decrease, with respect to the reference case, is 14% (B_W) and 13% (B_C). On the other hand, the duration of the final tailing zone become shorter as B_W is decreased or B_C is increased with percentage variations of about 36% (B_W) or 38% (B_C). The maximum devolatilization rate is increased by increasing B_W or decreasing B_C and is observed at shorter times. The maximum pressure always increases as the permeability, either for wood or char, decreased. The variations in the process dynamics do not introduce any significant variation in the yields of primary products. However, the activity of secondary reactions may be affected.

Deviations from the assumptions of local thermal equilibrium and release of the volatile products at the position where produced

To investigate the influences of the deviations from the assumptions of local thermal equilibrium between the solid and the gas/vapor phase, it is assumed that the volatile products are completely ($\alpha = 0$) or for the half ($\alpha = 0.5$) released at the location where they are produced (vs. the case of $\alpha = 1$

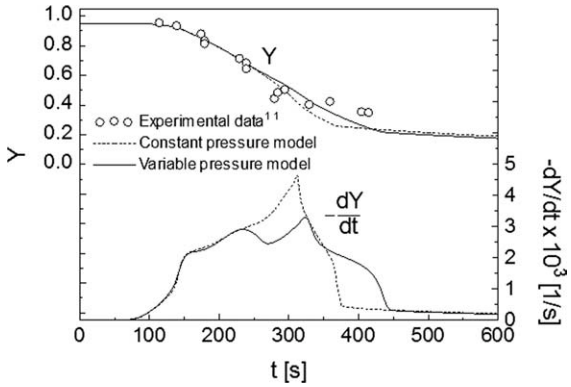

Figure 7. Predicted global mass fraction for the variable pressure model and the constant pressure model.

Predicted global mass fraction, *Y*, and time derivative of the mass fraction, $-dY/dt$, for the variable pressure model (solid lines) and the constant pressure model (dashed lines). Experimental data[11] (symbols) are included for comparison purposes.

Table 2. Predicted Process Parameters for the Variable Pressure Model (A) and the Constant Pressure Model (B)

Model	Y_C (wt %)	Y_G (wt %)	Y_T (wt %)	t_i (s)	t_{infl} (s)	t_c (s)	Y_{infl}	$dY_{vm} \times 10^3$ (s^{-1})	t_{vm} (s)	p_{max}/p_{atm}	$t_{p_{max}}$ (s)
A	14.8	7.7	72.3	145	446	544	0.21	3.50	326	5.2	153
B	15.0	7.6	72.4	146	375	596	0.26	4.68	312	–	–

Predicted yields of the three product classes (Y_C, Y_T, Y_G) expressed on a dry mass basis, induction time, t_i, defined as the time when a conversion 5% is reached, inflection time, t_{infl}, defined as the time when, after the absolute maximum, the slope changes of the rate of weight loss, and corresponding solid mass fraction, Y_{infl}, conversion time (conversion of 95%), t_c, maximum volatile release rate, dY_{vm}, and corresponding time, t_{vm}, and maximum relative pressure, p_{max}/p_{atm}, and corresponding time, $t_{p_{max}}$, for the variable pressure model (A) and the constant pressure model (B) (input data in Table 1).

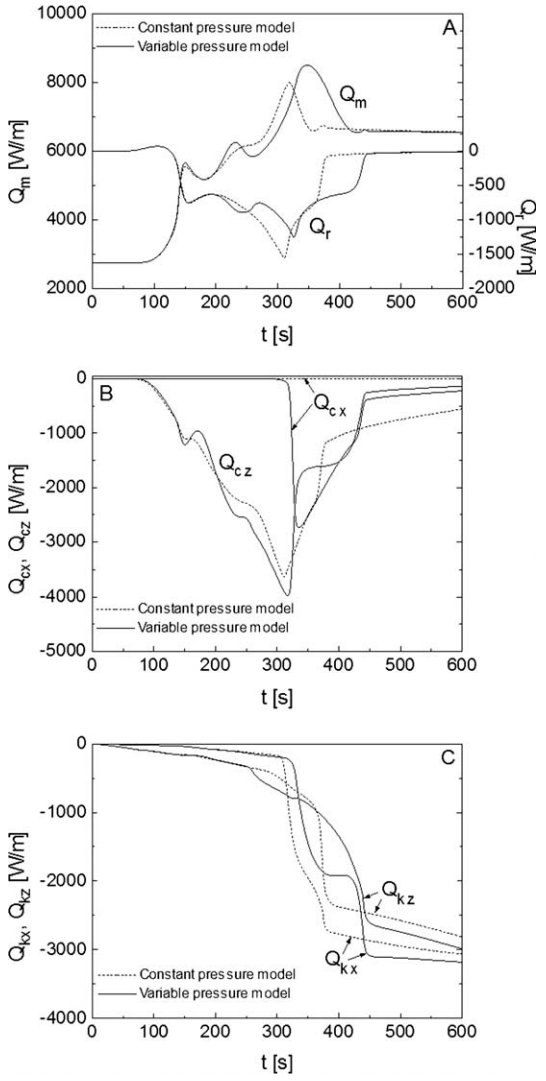

Figure 8. Contributions of the energy conservation equation integrated over the computational domain.

A: Contributions due to the reaction enthalpy, Q_r (Eq. 12), and the microwave energy term, Q_m (Eq. 13), of the energy conservation equation integrated over the computational domain (Eq. 7), as functions of time for the variable pressure model (solid lines) and the constant pressure model (dashed lines). **B**: Contributions due to convective heat transport along the x direction, Q_{cx} (Eq. 8), and the z direction, Q_{cz} (Eq. 9), of the energy conservation equation integrated over the computational domain (Eq. 7), as functions of time for the variable pressure model (solid lines) and the constant pressure model (dashed lines). **C**: Contributions due to conductive heat transport along the x direction, Q_{kx} (Eq. 10), and the z direction, Q_{kz} (Eq. 11), of the energy conservation equation integrated over the computational domain (Eq. 7), as functions of time for the variable pressure model (solid lines) and the constant pressure model (dashed lines).

of the reference case where there is local equilibrium between phases and the release of volatile products occurs from the external specimen surfaces). Results are discussed for the size/shape of the heated/reacted region by means of the color maps of temperature (Figure 9) and char density (Figure 10) for the cases of $\alpha = 0$ (Figures 1 and 2, which refer to the case of $\alpha = 1$, can be used for comparison). Furthermore, the weight loss curves are considered (Figure 11) together with a list of the main process parameters (Table 4) for $\alpha = 1$, 0.5, 0. The color maps of temperature for $\alpha = 0$ suggest that the conversion process is initiated in correspondence of the hot zone located at the lower part of the specimen. Then, the complete absence of convective preheating does not permit the attainment of temperatures sufficiently high in the hot upper zone for the reaction to begin. Thus, the reaction enlarges from the bottom hot zone with a rounded shape (vs. the stretched shape obtained for the case of $\alpha = 1$).

Independently from the α value, microwave-induced pyrolysis of a thick wood block is always characterized by the release of a large part (conversions of 80–90%) of the volatile products over a relatively narrow interval of time. However, for the case of $\alpha = 0$, apart from the quantitative differences, there are also two main qualitative differences, that is, the absence of the second local peak in the devolatilization rate, a consequence of the lack of convection and the onset of reaction in the second upper reaction zone, and the tailing zone. The process is much faster with the duration of the first and second zone in the weight loss characteristics reduced by about 27 and 54% with respect to the case of $\alpha = 1$. Because of the absence of the slow tailing zone, differences with the conversion times become even longer (64%). The simulation carried out for the case of $\alpha = 0.5$ shows an intermediate behavior.

The shorter duration of the conversion process as the parameter α decreases indicates that the heat needed to bring the volatile products from the temperature of their formation to that of the hotter already reacted or partially reacted solid is larger than that provided to the colder still unreacted wood while they are transported toward the external surfaces of the specimen. In other words, for α different from 1, volatile species are totally or in part released in the reaction chamber at temperatures around 575–650 K, in accordance with the reaction kinetics of wood,[3] so that the microwave energy is used to heat at much higher temperature only the solid residue whose mass is much lower than the initial mass with significant energy saving. Finally, it is important to notice that the yields of primary products also vary with an increase in the char yields as the conditions of local thermal equilibrium is approached (from about 10 to 15%). This is as a consequence of a progressively slower heating rate of the specimen.

Table 3. Predicted Process Parameters for Values of the Wood and Char Permeabilities, B_W and B_C, Decreased and Increased by a Factor of Five

Model	Y_C (wt %)	Y_G (wt %)	Y_T (wt %)	t_i (s)	t_{infl} (s)	t_c (s)	Y_{infl}	$dY_{vm} \times 10^3$ (s^{-1})	t_{vm} (s)	p_{max}/p_{atm}	$t_{p_{max}}$ (s)
A	14.8	7.7	72.3	145	446	544	0.21	3.50	326	5.2	153
$B_W \times 5$	14.8	7.7	72.3	145	404	558	0.23	4.10	310	2.9	150
$B_W/5$	14.8	7.6	72.3	144	467	530	0.20	3.23	344	9.9	153
$B_C \times 5$	14.8	7.6	72.3	145	466	527	0.20	3.18	340	4.6	153
$B_C/5$	14.7	7.6	72.2	145	408	562	0.23	4.03	311	6.2	149

Predicted yields of the three product classes (Y_C, Y_T, Y_G) expressed on a dry mass basis, induction time, t_i, inflection time, t_{infl}, and corresponding solid mass fraction, Y_{infl}, conversion time, t_c, maximum volatile release rate, dY_{vm}, and corresponding time, t_{vm}, and maximum relative pressure, p_{max}/p_{atm}, and corresponding time, $t_{p_{max}}$, (definitions as in Table 2) for the variable pressure model and input data in Table 1 (A) and for values of the wood and char permeabilities, B_W and B_C, decreased and increased by a factor of five.

Conclusions

This study presents some results of a detailed two-dimensional mathematical model for the unsteady heat- and mass-transfer equations coupled with a quasi-steady formulation of the electromagnetic field for a pyrolyzing wood block.

Independently from the assumptions made in the description of the various processes, detailed distributions of the field variables show a process initially controlled by volumetric heating with a wide reaction zone that continuously enlarges from the most internal region toward the external surface of the wood sample. The global weight loss characteristics show that the process consists of an induction stage, a zone of high rates of volatile product release leading to mass loss of about 75–80%, and a final tailing zone associated with the slower conversion rates of the most external zones. The microwave energy generation contribution is always dominant (and practically the sole mechanism for the

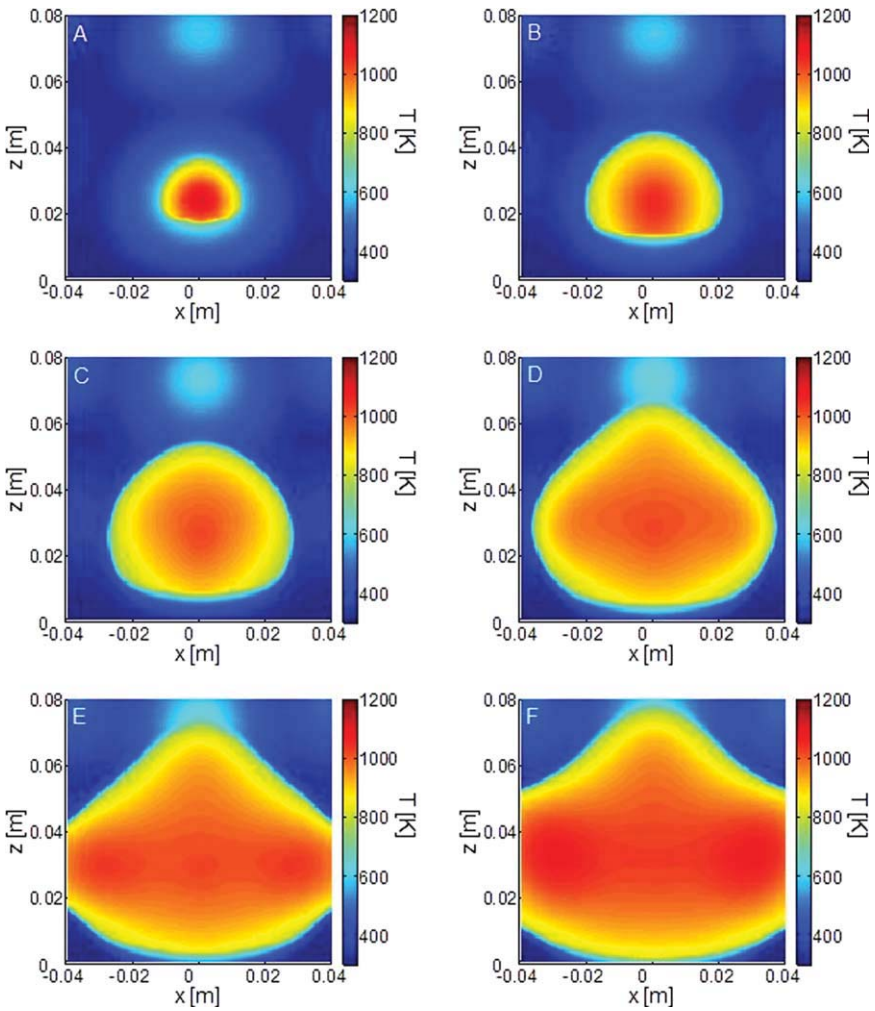

Figure 9. Color maps of temperature, *T*, at conversions of 5% (A, 107 s), 15% (B, 118 s), 30% (C, 136 s), 50% (D, 155 s), 65% (E, 166 s), 75% (F, 175 s) for the variable pressure model and $\alpha = 0$.

[Color figure can be viewed in the online issue, which is available at wileyonlinelibrary.com.]

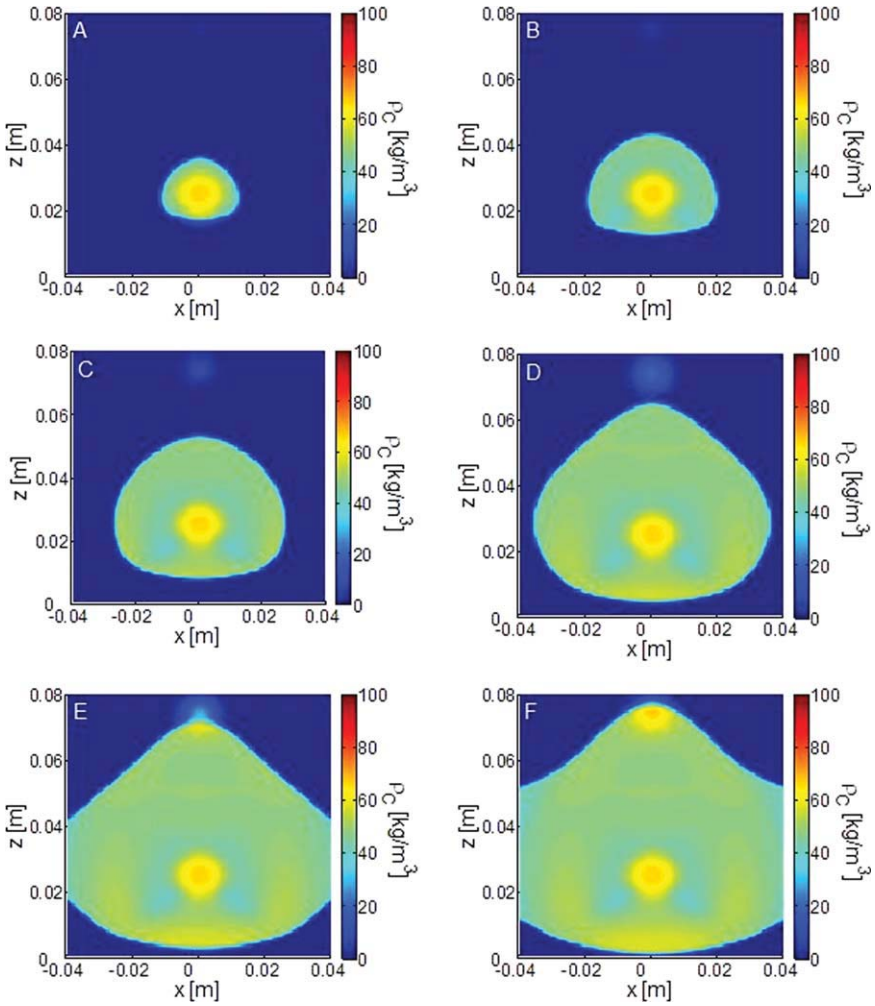

Figure 10. Color maps of char density, ρ_C, at conversions of 5% (A, 107 s), 15% (B, 118 s), 30% (C, 136 s), 50% (D, 155 s), 65% (E, 166 s), 75% (F, 175 s) for the variable pressure model and $\alpha = 0$.

[Color figure can be viewed in the online issue, which is available at wileyonlinelibrary.com.]

induction stage), but the second period is significantly affected by convective heat transfer. For the third period, conduction becomes the second most important heat-transfer mechanism.

The description of the flow field does not influence the process up to conversion of about 30%, essentially determined by the microwave energy generation and the properties of the specimen and the reaction chamber. The second stage of the process, where high rates of weight loss are established, is characterized by a longer duration (by about 31%) and a lower maximum volatile release rate (about 25%) for the two-dimensional and variable pressure model, as a consequence of a less effective distribution in the convective heating of the still unreacted wood region. Instead the duration of the last stage is shorter (by about 56%) owing to the presence of convective transport also across the wood fibers.

The detailed prediction of the process dynamics, including the Darcy law, reveals that the maximum pressure is quite high and is significantly dependent on the permeabilities of both wood and char. The flow of hot volatile products, for the large part of the conversion process, is directed along the wood fibers through a preferable route, that is, a channel,

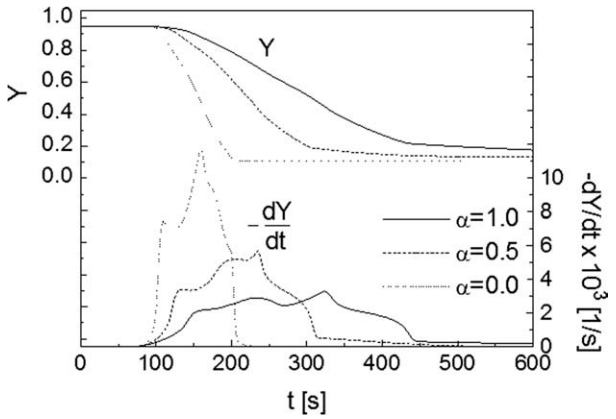

Figure 11. Predicted global mass fraction, *Y*, and time derivative of the mass fraction, $-dY/dt$, for the variable pressure model for $\alpha = 1$ (solid lines), $\alpha = 0.5$ (dashed lines) and $\alpha = 0$ (dotted lines).

Table 4. Predicted Process Parameters for the Variable Pressure Model and Values of the Parameter α =1 (Reference Case), 0.5, and 0

Model	Y_C (wt %)	Y_G (wt %)	Y_T (wt %)	t_i (s)	t_{infl} (s)	t_c (s)	Y_{infl}	$dY_{vm} \times 10^3$ (s^{-1})	t_{vm} (s)	p_{max}/p_{atm}	$t_{p_{max}}$ (s)
$\alpha = 1.0$	14.8	7.7	72.3	145	446	544	0.21	3.50	326	5.2	153
$\alpha = 0.5$	12.7	9.1	72.9	126	314	347	0.18	5.70	236	4.9	128
$\alpha = 0.0$	10.4	11.2	72.6	106	209	197	0.11	11.6	159	1.0	10

Predicted yields of the three product classes (Y_C, Y_T, Y_G) expressed on a dry mass basis, induction time, t_i, inflection time, t_{infl}, and corresponding solid mass fraction, Y_{infl}, conversion time, t_c, maximum volatile release rate, dY_{vm}, and corresponding time, t_{vm}, and maximum relative pressure, p_{max}/p_{atm}, and corresponding time, $t_{p_{max}}$, (definitions as in Table 2) for the variable pressure model and values of the parameter α =1 (reference case), 0.5 and 0.

located at the sample centerline. This feature, induced by pressure variation and resistance to mass flow, produces a stretched shape of the already reacted zone vs. the more rounded region of the simplified constant pressure model.

The analysis of the simulation results indicates that the introduction of a resistance to the flow of volatile species and linking the pressure and velocity variations via the Darcy law produces a more realistic distribution of the main process variables. Although no experimental evidence is currently available, the attainment of quite large pressures, as simulated by the model, most likely can lead to partial structural failure and/or the formation of fissures and cracks that are not described. However, as also testified by the good agreement between the model predictions and the measured weight loss curve, it can be thought that these structural modifications, in the real situation, do not modify significantly the direction of the gas flow from the direction of the medium fibers and also guarantee thermal equilibrium at each spatial position between the solid phase and the gas/vapor phase products.

Simulations show that deviations from the assumption of local thermal equilibrium with the release of volatile species at the location where they are produced highly affect the process whose duration is reduced. This means that the heat needed to bring the volatile products from the relatively low temperature of their formation to the high temperature of the already charred region is always much larger than the amount of heat provided by convective transport to the still cold and unreacted wood.

Finally, it is worth noting that unlike pyrolysis technologies based on conventional heating for the production of bio-oil or biochar, microwave-induced pyrolysis of wood is still in the initial stage. Hence, an improved knowledge of the process fundamentals can help in constructing the basis for technological design and development. On the other hand, although one of the main objectives of mathematical models is the application for process design and development, it is believed that further efforts are needed for such a purpose in the case of microwave pyrolysis. In the first place, the effects of the moisture content and evaporation on the dielectric properties of the medium should be described and investigated. Secondary reaction mechanisms should also be taken into account as, in practical situations, the activity of these reactions may not be negligible. In general, the use of detailed (vs. lumped) reaction mechanisms, capable of predicting the evolution of the main species formed, could also represent a formidable improvement.

Notation

A_1, A_2, A_3 = pre-exponential factors for the reactions of wood to tar (1), gas (2) and char (3) (1/s)
B = permeability (m^2)
d = pore diameter (m)
dY_{vm} = maximum volatile release rate [1/s)
$d\varepsilon^*_{co}$ = coefficient in the temperature-dependent law of char relative permittivity (1/K)
E_1, E_2, E_3 = activation energies for the reactions of wood to tar (1), gas (2) and char (3) (J/kmol)
F = waveguide depth (m)
f = frequency (1/s)
h_b = global heat-transfer coefficients for bottom surface. ($W/(m^2K)$)
h_g, h_s = specific enthalpy of the gas (g) and solid (s) phase. (J/kg)
K_1, K_2, K_3 = kinetic constant for the reactions of wood to tar (1), gas (2) and char (3) (1/s)
k = thermal conductivity (W/(mK))
k^* = effective thermal conductivity (W/(mK))
L = length in z-direction (m)
p = pressure (Pa)
P_0 = input power (W)
Q = local electromagnetic generation intensity (W/m^3)
T = temperture (K)
t = time (s)
t_c = conversion time (s)
t_i = induction time (s)
t_{infl} = inflection time (s)
$t_{p_{max}}$ = time of maximum pressure (s)
t_{vm} = time of maximum volatile release rate (s)
u = velocity along x-direction (m/s)
v = velocity along z-direction (m/s)
x = coordinate along cavity width (m)
Y = mass fraction
Y_{infl} = mass fraction at inflection time
W = length in x-direction (m)
z = coordinate along cavity height (m)
α = volatile fraction convected across the specimen
$\Delta h^0_1, \Delta h^0_2, \Delta h^0_3$ = heat of reaction of wood to tar (1), gas (2) and char (3) at standard conditions (J/kg)
$\Delta x, \Delta z$ = spatial grid step along the x and z directions (m)
ε^* = relative complex permittivity
η = conversion degree
μ = gas-phase viscosity (Pa s)
ρ = density (kg/m^3)
ϕ = porosity
ω = emissivity

Subscripts

0 = initial
atm = ambient
C = char
c = cavity
G = permanent gases
g = gas phase
I = incident plane
max = maximum
N_2 = nitrogen
S = sample
T = tar
x, z = coordinates along cavity width and height
W = wood
WG = waveguide

Literature Cited

1. Bridgwater AV, Peacocke GVC. Fast pyrolysis processes for biomass. *Renew Sustain Energy Rev*. 2000;4:1–73.
2. Antal MJ, Gronli MG. The art, science and technology of charcoal production. *Ind Eng Chem Res*. 2003;42:1619–1640.
3. Di Blasi C. Modeling chemical and physical processes of wood and biomass pyrolysis. *Prog Energy Combust Sci*. 2008;34:47–90.
4. Menendez JA, Arenillas A, Fidalgo B, Fernandez Y, Zubizarreta L, Calvo EG, Bermudez JM. Microwave heating processes involving carbon materials. *Fuel Process Technol*. 2010;91:1–8.
5. Zhang X, Hayward DO. Applications of microwave dielectric heating in environment-related heterogeneous gas-phase catalytic systems. *Inorg Chim Acta*. 2006;359:3421–3433.
6. Jones DA, Lelyved TP, Mavrofidis SD, Kingman SW, Miles NJ. Microwave heating applications in environmental engineering—a review. *Resour Conservat Recycl*. 2002;34:75–90.
7. Allan GG, Krieger-Brockett B, Work DW. Dielectric loss microwave degradation of polymers: cellulose. *J Appl Polym Sci*. 1980;25:1839–1859.
8. Chan RW, Krieger-Brockett B. Kinetics of dielectric-loss microwave degradation of polymers: lignin. *J Appl Polym Sci*. 1981;26:1533–1553.
9. Baysar A, Johnson KJ, Kuester JL. *Microwave heating applications in thermochemical biomass conversion*. In: Brigdwater AV, Kuester JL, editors. *Research in Thermochemical Biomass Conversion*. Barking, Essex, UK: Elsevier Science Publisher, 1988;680–695.
10. Krieger-Brockett B. Microwave pyrolysis of biomass. *Res Chem Intermediat*. 1994;20:39–49.
11. Miura M, Kaga H, Sakurai A, Kakuchi T, Takahashi K. Rapid pyrolysis of wood block by microwave heating. *J Anal Appl Pyrolysis*. 2004;71:187–199.
12. Menendez JA, Dominguez A, Fernandez Y, Pis JJ. Evidence of self-gasification during microwave induced pyrolysis of coffee hulls. *Energy Fuels*. 2007;21:373–378.
13. Dominguez A, Menendez JA, Fernanzez Y, Pis JJ, Nabais JMV, Carrot PJM, Carrot MMLR. Conventional and microwave induced pyrolysis of cofee hulls for the production of a hydrogen rich gas. *J Anal Appl Pyrolysis*. 2007;79:128–135.
14. Yu F, Deng S, Chen P, Liu Y, Wan Y, Olson A, Kittelson D, Ruan R. Physical and chemical properties of bio-oils from microwave pyrolysis of corn stover. *Appl Biochem Biotechnol*. 2007;136–140:957–970.
15. Chen M, Wang J, Zhang M, Chen M, Zhu X, Min F, Tan Z. Catalytic effects of eight inorganic additives on pyrolysis of pine wood sawdust by microwave heating. *J Anal Appl Pyrolysis*. 2008;82:145–150.
16. Budarin VL, Clark JH, Lanigan BA, Shuttleworth P, Breeden SW, Wilson AJ, Macquarrie DJ, Milkowski K, Jones J, Bridgeman T, Ross A. The preparation of high-grade bio-oils through the controlled, low temperature microwave activation of wheat straw. *Bioresour Technol*. 2009;100:6064–6068.
17. Wan Y, Chen P, Zhang B, Yang C, Liu Y, Lin X, Ruan R. Microwave-assisted pyrolysis of biomass: catalysts to improve product selectivity. *J Anal Appl Pyrolysis*. 2009;86:161–167.
18. Franca AS, Oliveira LS, Nunes AA, Alves CCO. Microwave assisted thermal treatment of defective coffee beans press cake for the production of adsorbents. *Bioresour Technol*. 2010;101:1068–1074.
19. Robinson JP, Kingman SW, Barranco R, Snape CE, Al-Sayeg H. Microwave pyrolysis of wood pellets. *Ind Eng Chem Res*. 2010;49:459–463.
20. Fernando S, Adhikari S, Chandrapal C, Murali N. Biorefineries: current status, challenges, and future direction. *Energy Fuels*. 2006;20:1727–1737.
21. www.nzherald.co.nz
22. Zielonka P, Gierlik E. Temperature distribution during conventional and microwave wood heating. *Holz Roh Werkst*. 1999; 57:247–249.
23. Zhao H, Turner IW. The use of a coupled computational model for studying the microwave heating of wood. *Appl Math Model*. 2000;24:183–197.
24. Rattanadecho P. The simulation of microwave heating of wood using rectangular wave guide: influence of frequency and sample size. *Chem Eng Sci*. 2006;61:4798–4811.
25. Perré P, Turner IW. The use of numerical simulation as a cognitive tool for studying the microwave drying of softwood in an over-sized waveguide. *Wood Sci Technol*. 1999;33:445–464.
26. Ciacci T, Galgano A, Di Blasi C. Numerical simulation of the electromagnetic field and the heat and mass transfer processes during microwave-induced pyrolysis of a wood block. *Chem Eng Sci*. 2010;65:4117–4133.
27. Vegh V, Turner IW, Zhao H. Effective cell-centered time-domain Maxwell's equations numerical solvers. *Appl Math Model*. 2005;29:411–438.
28. Mur G. Absorbing boundary conditions for the finite-difference approximation of the time-domain electromagnetic-field equations. *IEEE Trans Electromagn Compat*. 1981;23:377–382.
29. Perry RH, Green D. *Perry's Chemical Engineers' Handbook*, 6th ed. New York: Mc-Graw-Hill, 1985.
30. Gronli MG. A Theoretical and Experimental Study of the Thermal Degradation of Biomass. PhD Thesis. Trondheim, Norway: NTNU, 1996.
31. Gronli MG, Melaaen MC. Mathematical model for wood pyrolysis—comparison of experimental measurements with model predictions. *Energy Fuels*. 2000;14:791–800.
32. Kanury MA, Blackshear PJ. Some considerations pertaining to the problem of wood burning. *Combust Sci Technol*. 1970;1:339–356.
33. Bird RB, Stewart WE, Lightfoot EN. *Transport Phenomena*. New York: Wiley, 1960.
34. Sherwood TK, Pigford RL, Wilke CR. *Mass Transfer*. New York: McGraw-Hill, 1975.
35. Chabory A, de Hon BP, Schilders WHA, Tijhuis AG. Fast transform based preconditioners for 2D finite-difference frequency-domain-waveguides and periodic structures. *J Comput Phys*. 2008;227:7755–7767.
36. Zhao H, Turner I, Liu FW. Numerical simulation of the power density distribution generated in a multimode cavity by using the method of line technique to solve directly for the electric field. *IEEE Trans Microwave Theory Tech*. 1996;44:2185–2194.
37. Wagenaar BM, Prins W, van Swaaij WPM. Flash pyrolysis kinetics of pine wood. *Fuel Process Technol*. 1994;36:291–302.
38. Di Blasi C. Physico-chemical processes occurring inside a degrading two-dimensional anisotropic porous medium. *Int J Heat Mass Transf*. 1998;41:4139–4150.
39. Di Blasi C. Heat, momentum and mass transfer through a shrinking biomass particle exposed to thermal radiation. *Chem Eng Sci*. 1996;51:1121–1132.
40. Di Blasi C. Dynamic behaviour of stratified downdraft gasifiers.*Chem Eng Sci*. 2000;55:2931–2944.
41. Zubkova V, Prezdho V. Change in dielectric properties of some Australian coals during the processes of pyrolysis. *J Anal Appl Pyrolysis*. 2006;75:140–149.
42. Rath J, Walfinger HG, Steiner G, Krammer G, Barontini F, Cozzani V. Heat of wood pyrolysis. *Fuel*. 2003;82:81–91.
43. Galgano A, Di Blasi C. Modeling wood degradation by the unreacted-core-shrinking approximation. *Ind Eng Chem Res*. 2003;42:2101–2111.

Manuscript received Nov. 6, 2010, and revision received Jan. 26, 2011.